Supplemental Material

High Mobility and High Thermoelectric Power Factor in Epitaxial ScN Thin films Deposited with Plasma-assisted Molecular Beam Epitaxy

Dheemahi Rao[1,2,3,£], Bidesh Biswas[1,2,3,£], Eduardo Flores[4], Abhijit Chatterjee[1,2,3], Magnus Garbrecht[5], Yee Rui Koh[6], Vijay Bhatia[5], Ashalatha Indiradevi Kamalasanan Pillai[5], Patrick E. Hopkins[6,7,8], Marisol Martin-Gonzalez[4] and Bivas Saha[1,2,3]

[1]*Chemistry and Physics of Materials Unit, Jawaharlal Nehru Centre for Advanced Scientific Research, Bangalore 560064, India.*
[2]*International Centre for Materials Science, Jawaharlal Nehru Centre for Advanced Scientific Research, Bangalore 560064, India.*
[3]*School of Advanced Materials, Jawaharlal Nehru Centre for Advanced Scientific Research, Bangalore 560064, India.*
[4] *Instituto de Micro and Nanotecnologia, IMN-CSIC, C/ Isaac Newton 8, Tres Cantos, 28760 Madrid, Spain.*
[5]*Australian Centre for Microscopy and Microanalysis, The University of Sydney, Camperdown, NSW 2006, Australia.*
[6]*Department of Mechanical and Aerospace Engineering, University of Virginia, Charlottesville, VA 22904,USA*
[7] *Department of Materials Science and Engineering, University of Virginia, Charlottesville, Virginia 22904, USA.*
[8]*Department of Physics, University of Virginia, Charlottesville, Virginia 22904, USA*

1. Growth Details

The ScN thin films were deposited on 1cm × 1cm MgO substrates. The substrates were initially ultra-sonicated in acetone and methanol for 10 minutes respectively and loaded into the MBE machine. In the preparation chamber, thermal cleaning of substrates was performed by heating substrates at 600℃ for 60 minutes. Following the thermal cleaning, the substrates were transferred into the growth chamber and were heated to 800°C for 30 minutes, before cooling to the deposition temperature of 600°C. Liquid nitrogen was continuously circulated around the MBE growth chamber to keep the surface from overheating. The thickness of the deposited films was measured with cross-sectional SEM and the deposition rate was found to be ~ 2.5 nm/min.

2. Transmission Electron Microscopy

The scanning/transmission electron microscopy (S/TEM) images and energy-dispersive x-ray spectroscopy maps were recorded by using an image- and probe-corrected and monochromated Themis-Z 60-300 kV equipped with a high-brightness XFEG source and Super-X EDS detector system for ultra-high count rates, operated at 300kV. For STEM imaging and EDX mapping, the probe corrector was used to form a focused probe of 0.7 Å diameter. The Super-X EDX detector system enables the recording of high spatial resolution EDS maps. The EDS maps contain arrays of individual spectra as large as 4k × 4k pixel, and by color coding the elemental peak of the highest intensity for each spectrum/pixel is shown

in the map. EDS maps with total counts well above 1,000,000 have been recorded for quantification. Absorption correction and applying the k-factor method yields a precision of about 2-3 % atomic percent content in an area of known sample thickness at that count rates.

3. Scanning Electron Microscopy and Focused Ion Beam

SEM imaging and TEM lamella preparation was done with a Helios Hydra DualBeam Plasma FIB. Samples were coated with a 20 nm of Au to prevent charging prior to FIB. Plan view SEM images were taken at 5kV with SE detector. For TEM sample preparation, a 100 nm Pt+C protective cap was deposited with 5kV electron beam followed by a 1 μm Pt+C protective cap with a 12kV Xe beam. A 30 kV Xe beam at 60, 15 and 4nA was used for trenching and lift out. The TEM specimens were welded to Mo grids using Xe beam Pt welding. Thinning was achieved with tilt angles of ±1.5° with currents of 300 and 100pA. Final thinning was done with 30kV at 30pA, checking for electron transparency using a 5 kV electron beam with a SE detector. When the ROI was thin enough it was finally polished with 5kV at 30 and 10pA, checking for electron transparency using 2kV electron beam with a SE detector.

4. Structural Details

The low-magnification HAADF-STEM micrograph (see S1 (a)) shows that the inverse pyramids have a slightly higher growth rate than the normal pyramids and shows up as rectangular features on the surface as observed in plain-view SEM images. AFM image (see S2(b)) exhibit a surface roughness of 1.13 nm.

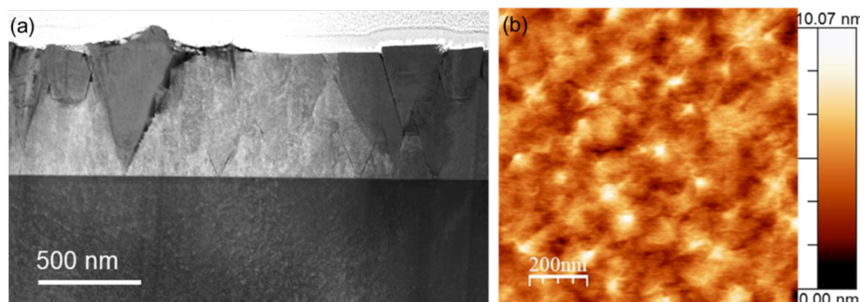

Figure S1: (a) STEM micrograph taken along the [010] direction of the ScN film on MgO substrate showing pyramid and inverse pyramid structures formed by the tilted grain boundaries in the ScN. The phase between the grain boundaries whose separation increases with thickness results in inverse pyramid like structure and are seen to grow taller than the surface. (b) AFM image showing plateau-pyramid structures on the surface of the film similar to the ones seen in plain view SEM (Fig. 3a). The surface roughness is calculated to be 1.13 nm.

4. Optical and Electrical Characterization

The optical absorption and bandgap of the MBE-deposited ScN thin films were measured with UV-visible spectroscopy measurements. Results showed that the ScN films exhibit and optical absorption coefficient of ~ 2×10^5 cm^{-1} that is comparable to the optical absorption exhibited by sputter deposited films. A plot of $(\alpha h\nu)^2$ *vs.* the incident photon energy exhibit ScN bandgap of 2.2 eV that is consistent with previous reports. It is also important to note

here that the uncertainty in Hall and thermoelectric measurements were small and remained within 3% of the reported values.

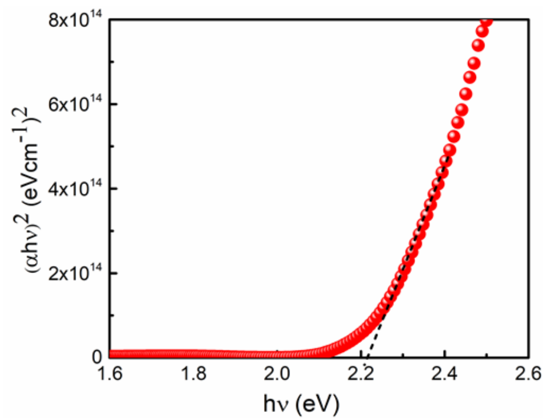

Figure S2: From the transmittance (T) and reflectance (R) data of the ScN films, absorption co-efficient was calculated using the formula $\alpha=\frac{1}{t}\ln\frac{(1-R)}{T}$ where t is the thickness of the film. The incident photon energy is plotted against $(\alpha h\nu)^2$ and the plot clearly shows the direct band gap of ScN at 2.2 eV.

Table 1: Room-temperature electronic properties of ScN thin films deposited with various methods are presented.

Deposition Technique	Substrate	Carrier concentration (cm^{-3})	Mobility (cm^2/V s)	Reference
MBE	MgO	8.6×10^{19}	127	*This work.*
	MgO	10^{19} to 10^{21}	50 - 130	*T. Ohgaki et al.*[1]
	GaN/SiC	10^{20}	20	*J. Casamento et al.* [2]
	Al_2O_3	10^{17}-10^{19}	1-10	*Moustakas et al.* [3]
	Al_2O_3	10^{19}-10^{21}	10-150	*T. Ohgaki et al.*[4]
Sputtering	MgO	2.5×10^{20}	106	*P.V.Burmistrova et al.* [5]
	MgO	4.4×10^{20} -1.5×10^{21}	50 - 70	*Cetnar et al* [6]
	MgO	10^{20}	18.6	*Saha et al.* [7]
	Al_2O_3	10^{21}	30	*Kerdsongpanya et al.*[8]
HVPE	Al_2O_3	0.9×10^{20}- 47×10^{20}	0.3 - 176	*Dismukes et al.*[9]
	Al_2O_3	3.7×10^{18}	284	*Y. Oshima et al.* [10]

5. Thermal Conductivity Measurement

The time-domain thermoreflectance (TDTR) is a well-known and proven technique in the nanoscale thermal conductivity measurements for the various thin film samples[11-14]. In this work, a two-color configuration TDTR is employed to characterize the thermal conductivity of the ScN thin films. The ScN thin films samples are coated with a ~ 80nm aluminum (Al) transducer for the optimum thermoreflectance coefficient in the measurements. The Ti:Sapphire femtosecond laser creates a train of the ~100fs short pulses with a wavelength of 800nm and 80MHz repetition frequency. The laser pulses are further split into a pump beam and probe beam. The probe laser wavelength is maintained with 800nm and pump laser is

converted into 400nm via a second harmonic crystal. The radii of the pump and probe laser beams were ~8μm and ~6μm respectively. Both laser beams power was limited to < 10mW during the measurements to prevent the overheating on the samples, which is an important step to avoid unwanted changes in the thermal property and the thermal diffusion model[15,16,17] fitting process. We also fixed the pump modulation frequency to a relatively high value, i.e. 8.8MHz in all the measurements to compensate to thin samples thicknesses. The experimental sensitivity plot (see below) suggest that the measurement sensitivity is dominated by the film's thermal conductivity as well as the Al/ScN interface thermal conductance.

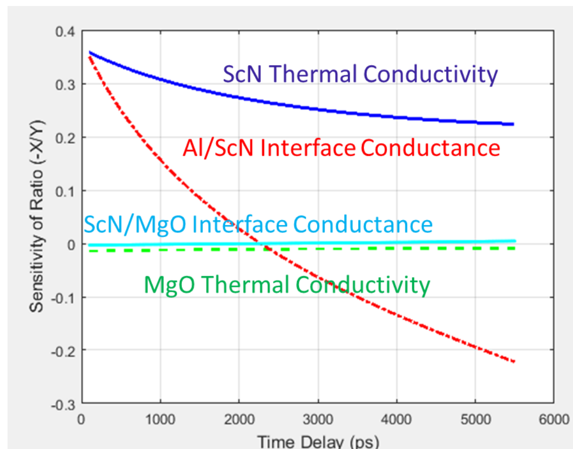

Figure S3: Sensitivity of Ration as a function of the time delay in TDTR measurement at 300K is presented that show that the measurement sensitivity is dominated by ScN's thermal conductivity as well as Al/ScN interface thermal conductance.

References

[1] T. Ohgaki, K. Watanabe, Y. Adachi, I. Sakaguchi, S. Hishita, N. Ohashi, and H. Haneda, J. Appl. Phys. **114**, (2013).
[2] J. Casamento, J. Wright, R. Chaudhuri, H. Xing, and D. Jena, Appl. Phys. Lett. **115**, (2019).
[3] Proceedings of the First Symposium on III-V Nitride Materials and Processes, edited by T. D. Moustakas, J. P. Dismukes, and S. J. Pearton (The Electrochemical Society Inc., Pennington, NJ, 1996), Vol. 96, p. 197.
[4] T. Ohgaki, I. Sakaguchi, N. Ohashi, and H. Haneda, J. Cryst. Growth **476**, 12 (2017).
[5] P. V. Burmistrova, J. Maassen, T. Favaloro, B. Saha, S. Salamat, Y. Rui Koh, M.S. Lundstrom, A. Shakouri, and T.D. Sands, J. Appl. Phys. **113**, (2013).
[6] J.S. Cetnar, A.N. Reed, S.C. Badescu, S. Vangala, H.A. Smith, and D.C. Look, Appl. Phys. Lett. **113**, (2018).
[7] B. Saha, G. Naik, V.P. Drachev, A. Boltasseva, E.E. Marinero, and T.D. Sands, J. Appl. Phys. **114**, (2013).
[8] S. Kerdsongpanya, N. Van Nong, N. Pryds, A. Žukauskaite, J. Jensen, J. Birch, J. Lu, L. Hultman, G. Wingqvist, and P. Eklund, Appl. Phys. Lett. **99**, 14 (2011).
[9] J.P. Dismukes, W.M. Yim, and V.S. Ban, J. Cryst. Growth **13–14**, 365 (1972).
[10] Y. Oshima, E.G. Villora, and K. Shimamura, J. Appl. Phys. **115**, (2014).

[11]Yee Rui Koh, MohammadAli Shirazi-HD, Bjorn Vermeersch, Amr M. S. Mohammed, Jiayi Shao, Gilles Pernot, Je-Hyeong Bahk, Michael J. Manfra, and Ali Shakouri, *Appl. Phys. Lett.* **109**, 243107 (2016)

[12] K. Aryana, J. T. Gaskins, J. Nag, J. C. Read, D. H. Olson, M. K. Grobis, and P. E. Hopkins, *Appl. Phys. Lett.* **116**, 043502 (2020)

[13]Yee Kan Koh, Myung-Ho Bae, David G. Cahill, and Eric Pop, *Nano Lett.* **10**, 4363–4368 (2010)

[14] Bivas Saha, Yee Rui Koh, Jonathan Comparan, Sridhar Sadasivam, Jeremy L Schroeder, Magnus Garbrecht, Amr Mohammed, Jens Birch, Timothy Fisher, Ali Shakouri, Timothy D Sands, *Phys. Rev. B* **93**, 045311 (2016)

[15] D. G. Cahill, *Rev. Sci. Instrum*. **75**, 5119 (2004)

[16] S. Dilhaire, J. M. Rampnoux, S. Grauby, G. Pernot, and G. Calbris, in *ASME 2009 Second International Conference on Micro/Nanoscale Heat and Mass Transfer* (2009), Vol. 2, pp. 451–456.

[17] Aaron J Schmidt, Xiaoyuan Chen, Gang Chen, *Rev. Sci. Instrum*. **79**, 114902 (2008)